DOI: https://doi.org/10.14311/TPFM.2026.030

DIRECT NUMERICAL SIMULATION OF CONTACT DYNAMICS IN PSEUDO-2D FLUIDIZED BEDS: EFFECTS OF SAMPLING DEPTH AND REGION SIZE

O. Studeník [1,2], J. Terpáková [1,3], J. Haidl [4], M. Isoz [1,3]

[1] Czech Academy of Sciences, Institute of Thermomechanics, Dolejškova 5, Prague 182 00, Czech Republic

[2] Department of Chemical Engineering, Faculty of Chemical Engineering, University of Chemistry and Technology, Technická 5, Prague 166 28, Czech Republic

[3] Department of Mathematics, Informatics and Cybernetics, Faculty of Chemical Engineering, University of Chemistry and Technology, Technická 5, Prague 166 28, Czech Republic

[4] Institute of Hydrology of the Czech Academy of Sciences, Pod Patankou 5, Prague 166 12, Czech Republic

Abstract

Fluidized-bed configurations are widely employed in industrial processes such as drying, granulation, and heterogeneous chemical reactions due to their efficient mixing and enhanced heat transfer. However, the description of such complex systems is predominantly based on empirical correlations derived from experimental data, which remain challenging to apply to non-standard conditions, such as systems with non-spherical particles or small and atypical geometries. An alternative approach is particle-resolved direct numerical simulation, employing computational fluid dynamics (CFD) coupled with the discrete element method (DEM) via the immersed boundary method (IBM). This high-fidelity approach enables detailed characterization of fluidized bed properties, including collision frequencies and three-dimensional granular temperature. In this contribution, we present the simulation results for a pseudo-2D fluidized bed, which also benefits from well-documented experimental data. Furthermore, we investigate the effects of sampling region size and depth on the evaluated properties, demonstrating a systematic approach for quantitative comparison between numerical simulations and experimental results.

Keywords: PR-DNS, CFD-DEM, Immersed boundary method, Fluidized beds, Granular temperature.

1 Introduction

The vast spread of systems containing solids dispersed within a fluid phase range from natural phenomena, such as sediment re-suspension [1] and blood flow [2], to man-made processes, including sedimentation columns and fluidized beds [3]. Fluidized bed apparatuses are commonly used in industrial applications such as polymerization, granulation, and particle drying [3]. Furthermore, the fluidized beds benefit from efficient mixing, thereby enhancing heat and mass transfer; albeit, at the cost of the system being *chaotic* and lacking analytical description. Consequently, generally applied descriptions are empirical correlations based on experimental data, which do not generalize well with respect to particle shape or device geometry. This, in turn, hinders optimization efforts for the industrial process as such efforts are, due to the missing general model, typically conducted through trial and error. To overcome these limitations, an alternative approach using high-fidelity numerical models may provide key insights for optimization.

High-fidelity numerical models offer multiple options for describing the behavior of fluidized beds or suspension flows in general, while each option strikes a specific balance between computational cost and result accuracy. Key factors to consider, apart from the model scale, are strategies for modeling underlying physical mechanism, such as (i) volume forces, (ii) particle-fluid interactions, and (iii) particle-particle/particle-boundary interactions [4]. Individual approaches vary in the treatment of the listed mechanisms.

For example, mixture models (MM) offer low computational cost when assuming sufficiently small volume fractions of dispersed particles, so that the whole system is described with a single momentum equation within the Eulerian framework [5]. This comes at the cost of treating volume forces via closure relations and leaving unresolved particle interactions. A more precise representation can be obtained using two-fluid models (TFMs), which describe both the fluid and the solids as interpenetrating Eulerian continua, each governed by its own set of equations. This model relies predominantly on closure relations, following kinetic theory for granular flows [6], thus hindering its calibration for high solid fractions and nonspherical particle shapes.

At the opposite end of the spectrum are particle-resolved direct numerical simulation (PR-DNS) models, whose standard implementations use the discrete element method (DEM) for particle tracing and collision treatment and computational fluid dynamics (CFD) for direct numerical simulation of fluid flow. Fluids and solids are typically coupled via a variant of the immersed boundary method (IBM) [7, 8]. Such models typically achieve high accuracy but are constrained by computational costs.

While PR-DNS models are not suitable for large-scale problems, they might be used to model a section of the device, in this case a fluidized bed, to obtain large-scale properties such as collision frequency or granular temperature, applicable for calibration of TFMs. To accomplish this goal, validation of PR-DNS results is required. Therefore, in this contribution, we will use the in-house developed PR-DNS solver OpenHFDIB-DEM [9, 10] to simulate a section of pseudo-2D fluidized bed. Since this configuration benefits from well-documented experimental data [11], it enables us to develop a methodology to evaluate key parameters: solid volume fraction, collision frequency, and granular temperature. Furthermore, we investigate the effects of sampling region size and depth on the obtained data.

2 Mathematical model

Let us first present the fundamentals of the applied PR-DNS model, the OpenHFDIB-DEM project. The project is a monolithic code that combines CFD and DEM methods via IBM, implemented as an extension to the OpenFOAM library [12]. For the system of gas-solid fluidized bed comprising spherical particles. A Newtonian fluid is considered with the assumption of incompressible flow. Thus, the fluid governing equations are written as

$$\underbrace{\frac{\partial \boldsymbol{u}}{\partial t} + \nabla \cdot (\boldsymbol{u} \otimes \boldsymbol{u}) - \nabla \cdot (\nu \nabla \boldsymbol{u})}_{\mathcal{M}(\boldsymbol{u})} = -\nabla \tilde{p} + \boldsymbol{g} + \boldsymbol{f}_{\text{ib}}\,, \quad \nabla \cdot \boldsymbol{u} = 0\,, \tag{1}$$

where ν kinematic viscosity, $\tilde{p}$ kinematic pressure, $\boldsymbol{u}$ is the fluid velocity, and $\boldsymbol{g}$ the graviational acceleration. The forcing term $\boldsymbol{f}_{\text{ib}}$ is induced by the immersed boundary and constructed to impose the presence of the solids onto the surrounding fluid.

The computational domain is $Q = I \times \Omega$ with I being the simulation time span and $\Omega \subset \mathbb{R}^3$ representing the spatial geometry of solved problem. Each individual particle is projected into Ω using the color function λ, denoting whether the part of the domain is a fluid (Ω_f), solid (Ω_s) or fluid-solid interface (Γ_sf), with moving particle velocity denoted as $\boldsymbol{u}_\text{ib}$. The forcing term and the color function can be defined as

$$\boldsymbol{f}_{\text{ib}} = \text{ceil}(\lambda) \hat{\boldsymbol{f}}_{\text{ib}}\,, \quad \hat{\boldsymbol{f}}_{\text{ib}} = \mathcal{M}(\boldsymbol{u}_{\text{ib}}) + \nabla \tilde{p} - \boldsymbol{g}\,, \quad \lambda = \begin{cases} 0 & \text{in} \quad \Omega_\text{f} \\ 1 & \text{in} \quad \Omega_\text{s} \\ (0,1) & \text{in} \quad \Gamma_\text{sf} \end{cases}\,, \tag{2}$$

with $\hat{\boldsymbol{f}}_{\text{ib}}$ being the immersed velocity-induced forcing defined in Ω. In the context of (2), $\boldsymbol{f}_{\text{ib}}$ is the restriction of $\hat{\boldsymbol{f}}_{\text{ib}}$ on $\Omega_\text{s} \cup \Gamma_\text{sf}$ via the λ field.

Fluid governing equations (1) are discretized via the finite volume method (FVM) and solved in a segregated iterative manner, using the PIMPLE Loop [13]. For further details regarding this specific IBM implementation, the reader is referred to works Municchi and Radl [7], Isoz et al. [9].

The behavior of the particles forming Ω_s is then described by DEM, the Lagrangian framework governed by Newton's second law of motion. For each solid (body $\mathcal{B}_i$) present within Q, the governing equations for its translational and rotational motion can be given as,

$$m_i \frac{\text{d}^2 \boldsymbol{x}_i}{\text{d}t^2} = \boldsymbol{f}_i^\text{g} + \boldsymbol{f}_i^\text{d} + \boldsymbol{f}_i^\text{c}\,, \quad I_i \frac{\text{d}\boldsymbol{\omega}_i}{\text{d}t} = \boldsymbol{t}_i^\text{d} + \boldsymbol{t}_i^\text{c}\,, \tag{3}$$

where m_i represents the mass of $\mathcal{B}_i$, $\boldsymbol{x}_i$ its centroid position, $\boldsymbol{\omega}_i$ its angular velocity and I_i is the matrix of its inertial moments at time t. The $\boldsymbol{f}$ and $\boldsymbol{t}$ denote, in order, forces and torques acting on $\mathcal{B}_i$. In the present contribution, the sources considered are gravity/buoyancy, drag, and collision forces, denoted by superscripts "g", "d", and "c", respectively.

The drag and gravity induced interactions on the right-hand side of equations (3) are computed as

$$\boldsymbol{f}_i^\text{d} = \int_{\mathcal{B}_i} \lambda\, \rho_\text{f}\, \boldsymbol{f}_{\text{ib}}\, dV\,, \quad \boldsymbol{t}_i^\text{d} = \int_{\mathcal{B}_i} \lambda\, \rho_\text{f}\, (\boldsymbol{x} - \boldsymbol{x}_i) \times \boldsymbol{f}_{\text{ib}}\, dV\,, \boldsymbol{f}_i^\text{g} = m_i\, \boldsymbol{g} \left(1 - \frac{\rho_\text{f}}{\rho_\text{s}^{\mathcal{B}_i}}\right)\,, \tag{4}$$

where ρ_f and $\rho_\text{s}^{\mathcal{B}_i}$ are the densities of the fluid and $\mathcal{B}_i$, respectively.

The treatment of contact forces and torques employs a soft-DEM approach that evaluates contact interactions based on the magnitude of solid-solid overlap and material properties of individual bodies, namely the Young modulus Y, Poisson ratio ν_p, coefficient of restitution ε and coefficient of friction μ. Due to the complex nature of the contact treatment implementation, which is out of scope of this contribution, the reader is referred to Studenik et al. [10].

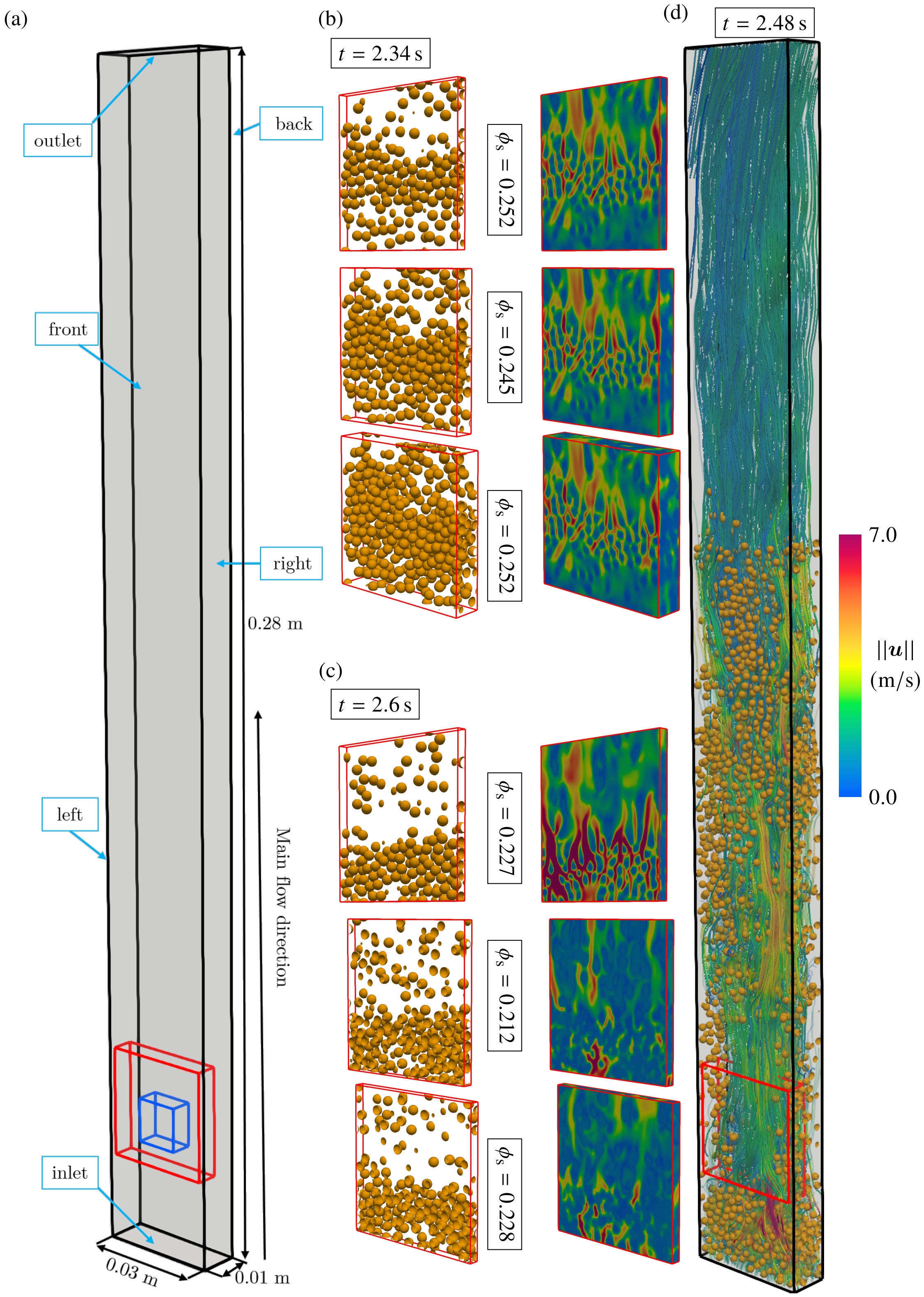

Figure 1: (a) Outline of computational domain with two types of sampling boxes highlighted. (b) Sampling boxes of side 15 d_p and depths of 1 d_p, 2 d_p, and 3 d_p; visualization of particles, solid volume fraction, and velocity contours at t = 2.34 s are shown. (c) Same as (b) but for boxes 0 d_p, 1 d_p, and 2 d_p away from the column front, and at time t = 2.60 s. (d) Full view of the simulated column at t = 2.48 s.

3 Simulation setup

In this work, we aim to create a digital twin of the experiment presented in work by Jiang et al. [11]. The experimental pseudo-2D fluidized bed has a hexahedral shape with dimensions of (0.3 m × 1 m × 0.02 m). Particles used had an average sphericity of 0.96 with a diameter $d_\mathrm{p} = 1.8$ mm, and a density $\rho_\mathrm{s} = 945\,\mathrm{kg/m^3}$. The total particle mass was 0.5 kg, which corresponds to 173 350 particles within the device. The fluidizing gas used was air and the device operated at a temperature of 20 °C and atmospheric pressure $p_\mathrm{atm} = 101.325$ kPa, leading to a density of $\rho_\mathrm{f} = 1.2\,\mathrm{kg/m^3}$ and viscosity $\nu = 1.5 \cdot 10^{-5}\,\mathrm{m^2/s}$. Such a system has a fluidization threshold estimated at $\boldsymbol{u}_\mathrm{mf} = (0,\ 0.56,\ 0)$ m/s. The experimental data are available for three superficial velocities expressed as $2\boldsymbol{u}_\mathrm{mf}$, $2.5\boldsymbol{u}_\mathrm{mf}$, and $3\boldsymbol{u}_\mathrm{mf}$ but this contribution is focused solely on $2.5\boldsymbol{u}_\mathrm{mf}$.

Because our focus is on the PR-DNS approach for simulating the experiment presented, the computational costs would be prohibitive. Therefore, to simulate the presented device, the simulation scale is reduced to (0.03 m × 0.28 m × 0.01 m). To compensate for the reduced dimensions, the sides are prescribed with cyclic boundary conditions and the back is prescribed with symmetry boundary conditions. Therefore, in theory, the dimensions of the system should correspond to (∞ m × 0.28 m × 0.02 m). The system outline is depicted in Figure 1, and boundary conditions are listed in Table 1. Furthermore, the particles are modeled as perfect spheres with material properties of $Y = 50$ MPa, $\nu_\mathrm{p} = 0.5$, $\varepsilon = 0.75$, $\mu = 0.1$. The system contains 2 200 particles, corresponding to $1/4^\mathrm{th}$ of static bed height for the experiment.

Field / Patch	p	λ	$\boldsymbol{u}$	$\boldsymbol{f}_\mathrm{ib}$
inlet	$\boldsymbol{n}\cdot\nabla p = 0$	$\boldsymbol{n}\cdot\nabla\lambda = 0$	$\boldsymbol{u} = 2.5\,\boldsymbol{u}_\mathrm{mf}$	$\boldsymbol{n}\cdot\nabla\boldsymbol{f}_\mathrm{ib} = \boldsymbol{0}$
outlet	$p = p_\mathrm{atm}$	$\boldsymbol{n}\cdot\nabla\lambda = 0$	$\boldsymbol{n}\cdot\nabla\boldsymbol{u} = \boldsymbol{0}$	$\boldsymbol{n}\cdot\nabla\boldsymbol{f}_\mathrm{ib} = \boldsymbol{0}$
left/right	cyclic	cyclic	cyclic	cyclic
front	$\boldsymbol{n}\cdot\nabla p = 0$	$\boldsymbol{n}\cdot\nabla\lambda = 0$	$\boldsymbol{u} = \boldsymbol{0}$	$\boldsymbol{n}\cdot\nabla\boldsymbol{f}_\mathrm{ib} = \boldsymbol{0}$
back	symmetry	symmetry	symmetry	symmetry

Table 1: Boundary conditions used in the simulation.

The spatial domain Ω for the problem is prepared to consist of uniform hexahedral cells. The following discretization schemes were selected for the simulation: for time integration, the Crank-Nicolson method with an off-centering factor of 0.75; the convective term was treated using the MinMod scheme; the remaining numerical schemes were second order. With the uniform cartesian mesh, no non-orthogonal corrections were applied. Hence, simulation was ran with almost 2^nd order accuracy for both spatial and temporal discretization.

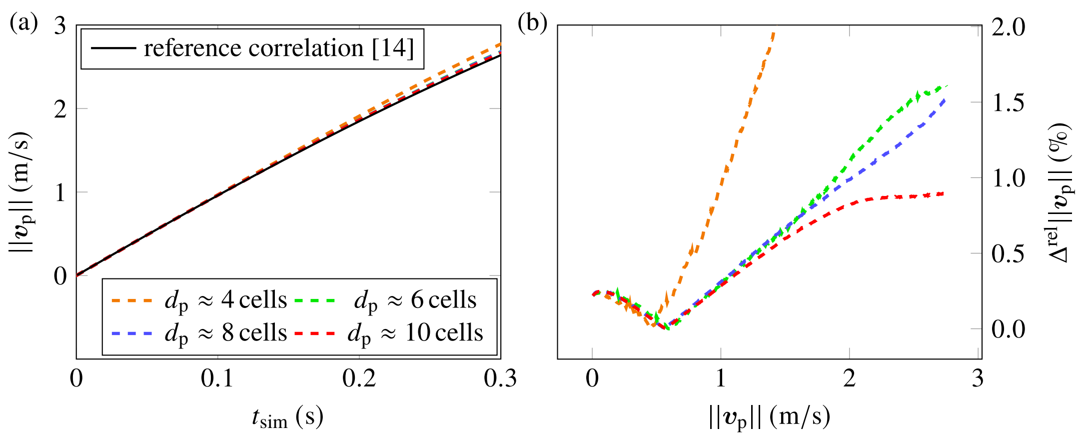

Figure 2: Effect of mesh resolution on the settling of a single particle in air. (a) Particle velocity magnitude for different mesh resolutions relative to particle diameter. (b) Relative error of the velocity magnitude with respect to the correlation [14].

To determine a suitable mesh resolution, a simplified test of a single particle settling was conducted. The fluid and solid properties were the same as for the main simulation and mesh resolutions of {4, 6, 8, 10}

FVM cells per particle diameter were tested. The obtained particle velocities as well as their difference from the correlation available for this simplified case are given in Figure 2 The mesh resolution of 8 FVM cells per particle seems to provide the best trade-off between simulation accuracy and computational time. Using this resolution yields the cell size of 225 μm, the mesh with 7.2 million cells, and differences in particle velocity between our model and the correlation below 1.5 % for the whole range of velocities of interest..

To compare the final simulation results with experimental data, data-collection zones are prescribed throughout the domain. Each zone is used to record the number of particles within (N_p), the number of collisions (N_c), and the solid fraction (ϕ_s). Consequently, the collision frequency (f_c) and the square root of granular temperature ($\sqrt{\Theta_{2D}}$), which in this setting corresponds to pseudo-2D granular temperature from [11], can be calculated as

$$f_c = \frac{N_c}{N_p\,\Delta t}, \qquad \sqrt{\Theta_{2D}} = \frac{5\sqrt{\pi} d_p f_c}{36\phi_s}\left(1 - \left(\frac{\phi_s}{\phi_{s,\max}}\right)^{1/3}\right), \tag{5}$$

where $\phi_{s,\max}$ is maximum solid fraction for random packed bed [15]; for further details see [11].

With respect to the sizes of the zones, we follow [11] and use boxes of depth 1 d_p and side 6 d_p (marked "*a*") and of side 15 d_p ("*b*"), see Figure 1a. While [11] also used boxes of side 45 d_p ("*c*"), this largest measured box does not fit into our simulation domain. Furthermore, while [11] was, due to measurability, always limited to the box depth of 1 d_p and boxes adjacent to the column front wall ("f"), we also take into account data from boxes 2 d_p and 3 d_p deep; see Figure 1b and from boxes of the depth 1 d_p but 1 d_p and 2 d_p away from the front wall; see Figure 1c. Finally, to fully leverage the simulation capabilities, the sampling boxes are placed from the inlet to the outlet in steps of 3 d_p, ensuring full coverage of the domain.

4 Simulation results

The simulation was evaluated using 48 cores of an HPC server with the total of 192 cores split between two 4$^{\text{th}}$ generation AMD EPYC$^{\text{TM}}$ 9654 96-core processors and with 1.5 TB RAM memory. To simulate 1 s of the flow required approximately 3.5 weeks due to limitations imposed by the CFL condition. The qualitative results for this simulation are displayed in Figure 1b-d. The velocity profile of the modeled bed is shown in Figure 3, demonstrating that no particle exceeds a velocity of 1.7 m/s and highlighting the chaotic manner of the fluidized bed where the velocity of the particles changes every moment.

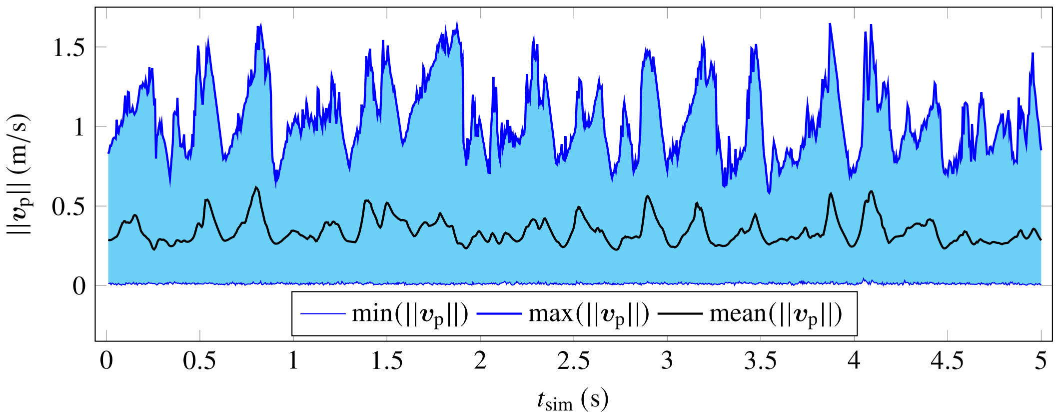

Figure 3: The profile of particle velocities recorded during the simulation, displaying average particle velocity and the range in which particles move during the simulation.

Nevertheless, the main focus of this contribution is the collision frequency, the granular temperature, and the solid volume fraction sampled within the predefined zones, and the influence of the zones' size, depth, and position on the properties studied. First, in Figure 4, we study the temporal evolution of ϕ_s and f_c in boxes placed ≈ 3 cm above the inlet. Specifically, the effect of sampling zone size 6 d_p ("*a*") vs. 15 d_p ("*b*") is compared in Figure 4a. It can be seen how using a bigger sampling regions smoothens ϕ_s and allows for higher peaks in f_c. Next, in Figure 4b, influence of the 15 d_p ("*b*") zone thickness on the results is shown. Further smoothening of ϕ_s can be seen when going from 1 d_p to 1 d_p deep zone but between 2 d_p and 3 d_p, there is almost no difference. Finally, in Figure 4c, we examine the effect of distance of the "a" type region from the column front wall. There, see that both ϕ_s and f_c smoothen with increasing distance of the sampling zone from wall.

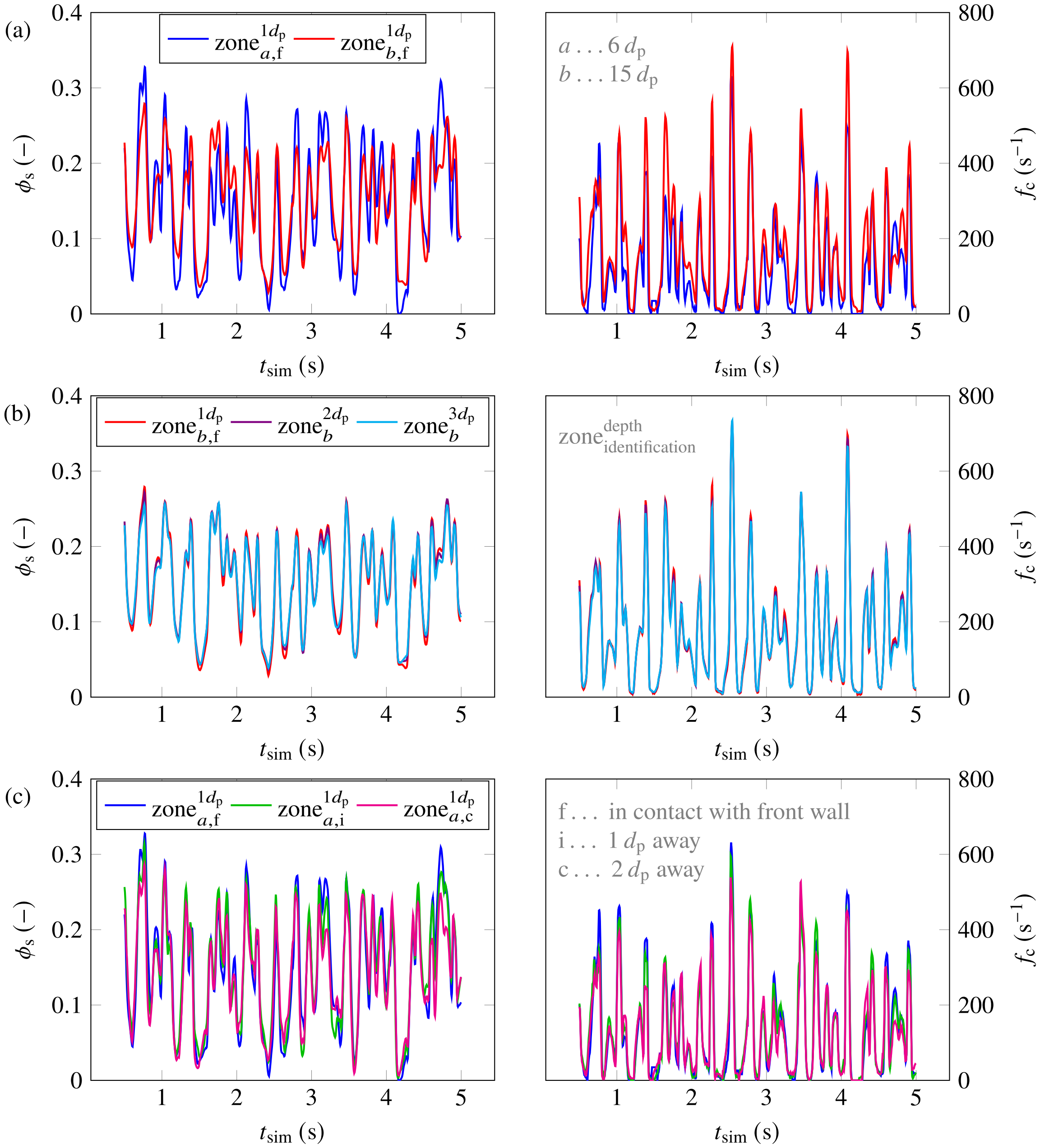

Figure 4: Temporal evolution of solid volume fraction ϕ_s and collision frequency f_c from data collection zones with center positioned 0.03 m above the inlet. (a) Effect of sampling region size on the front zone with 1 d_p depth. (b) Effect of sampling zone depth. (c) Effect of zone distance from front wall.

The performed study of the time-resolved data showed a relatively high robustness of the results with respect to the sampling zone depth and positioning. However, increasing the region size leads to increased peaks in f_c and decreased peaks in ϕ_s. Examining (5), it can be seen that such a behavior should also lead to an increase in observed granular temperature $\sqrt{\Theta_{2D}}$. Moreover, to be able to compare our simulation results to experiments [11], we compute temporal averages of the tracked data in all available sampling zones. The results are given in Figure 5.

First, note that the computational domain presented is too small to contain the sampling zone of size of 45 d_p (”c”) and the simulation data presented in Figure 5 for the collision frequency are extrapolated

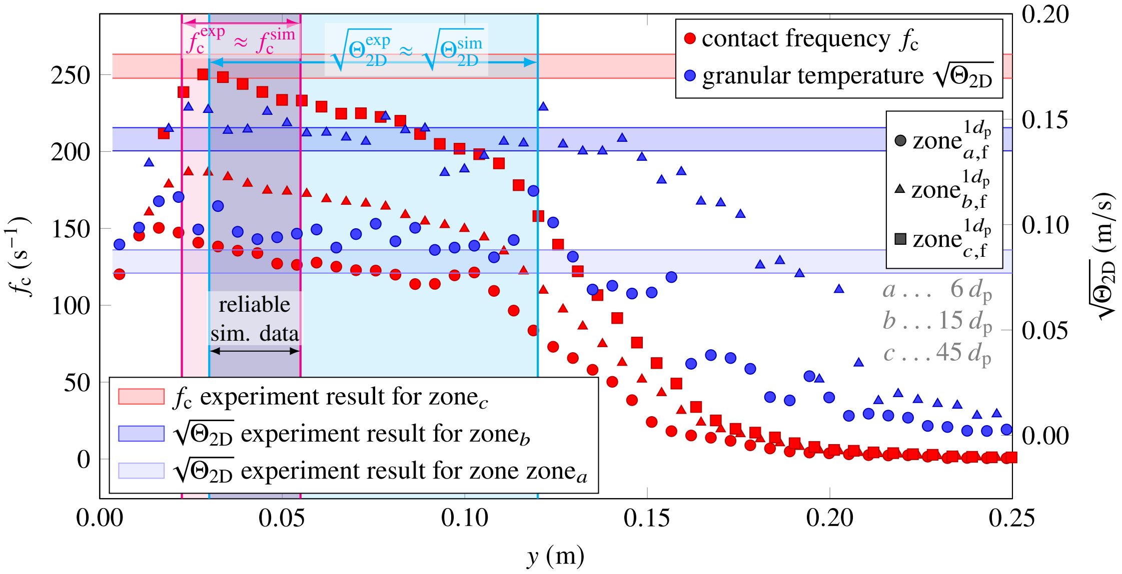

Figure 5: The time-averaged collision frequency and square root of granular temperature along the height of the computational domain. Simulation results are compared to experimental ranges reported in Appendix B of [11]. Areas of acceptable agreement between simulation and experiment in f_c and $\sqrt{\Theta_{2D}}$ are highlighted in magenta and cyan, respectively, and used to identify vertical position in Ω that corresponds to "high-level" locations in [11].

based on the ratio of the results for regions a and b. Next, the experimental results depicted correspond to "high-level" locations in [11] as our system is too small to have any relevance for the "low-level" locations studied in the aforementioned article. Finally, examining the agreement between measured and estimated collision frequency and granular temperature, we were able to identify a zone in which there is a good agreement between simulation and experiment and where the detailed simulation data can be used to extend the measured dataset. This zone ranges from 0.03 m to 0.055 m above the inlet for the zone centers and is highlighted in the Figure 5.

5 Conclusions

The present contribution focuses on the development of a digital twin for a pseudo-2D fluidized-bed experiment using the PR-DNS approach. Using the OpenHFDIB-DEM project within the OpenFOAMv8 library. The simulation results were studied in a similar manner as its experimental counterpart. The predefined zones across the simulation domain were used to evaluate collision frequency, solid volume fraction, and the square root of granular temperature. These results were studied in regard to the zone size, thickness, and position. The result confirm trend between region size and collision frequency. Furthermore, time-averaged data for each zone along the simulated column height were compared with experimental data. This comparison allowed us to identify a zone in our simulation in which the numerical data can be used to bring new insights into the fluidized bed behavior. In the future, we will also study this system at other gas inlet velocities and used the combined data to (i) further validate OpenHFDIB-DEM, (ii) calibrate two-fluid models for fluidization with high solid phase volume fractions, and (iii) validate the assumptions made to process the experimental data.

Acknowledgment

This research was co-funded by the European Union under the project Metamaterials for thermally stressed machine components (reg. no. CZ.02.01.01/00/23_020/0008501). The work was financially supported by the institutional support RVO:61388998, and by the grant project with No. 25-17815S of the Czech Science Foundation of the Czech Republic.

References

[1] M. O. Green and G. Coco, “Review of wave-driven sediment resuspension and transport in estuaries,” *Reviews of Geophysics*, vol. 52, no. 1, pp. 77–117, 2014.

[2] C. Porcaro and M. Saeedipour, “Unresolved RBCs: An upscaling strategy for the CFD-DEM simulation of blood flow with deformable cells,” *Computers in Biology and Medicine*, vol. 181, p. 109081, 2024.

[3] E. Zhalehrajabi, K. K. Lau, T. Hagemeier, and A. Idris, “Evaluation of hydrodynamic behavior of urea granules in a pseudo-2D fluidized bed using drag models and comparison with piv technique,” *Powder Technology*, vol. 406, p. 117578, 2022.

[4] F. Alobaid, N. Almohammed, M. Massoudi Farid, J. May, P. Rossger, A. Richter, and B. Epple, “Progress in CFD simulations of fluidized beds for chemical and energy process engineering,” *Progress in Energy and Combustion Science*, vol. 91, p. 100930, 2022.

[5] G. Tronci, A. Buffo, M. Vanni, and D. Marchisio, “Validation of the diffusion mixture model for the simulation of bubbly flows and implementation in OpenFOAM,” *Computers & Fluids*, vol. 227, p. 105026, 2021.

[6] D. Gidaspow, *Multiphase Flow and Fluidization*. Academic Press, 1994.

[7] F. Municchi and S. Radl, “Consistent closures for Euler-Lagrange models of bi-disperse gas-particle suspensions derived from particle-resolved direct numerical simulations,” *International Journal of Heat and Mass Transfer*, vol. 111, pp. 171–190, 2017.

[8] B. Blais, M. Lassaigne, C. Goniva, L. Fradette, and F. Bertrand, “A semi-implicit immersed boundary method and its application to viscous mixing,” *Computers & Chemical Engineering*, vol. 85, pp. 136–146, 2016.

[9] M. Isoz, M. Kotouc Sourek, O. Studenok, and P. Koci, “Hybrid fictitious domain-immersed boundary solver coupled with discrete element method for simulations of flows laden with arbitrarily-shaped particles,” *Computers & Fluids*, vol. 244, 2022.

[10] O. Studenik, M. Isoz, M. Kotouc Sourek, and P. Koci, “OpenHFDIB-DEM: An extension to OpenFOAM for CFD-DEM simulations with arbitrary particle shapes,” *SoftwareX*, vol. 27, 2024.

[11] Z. Jiang, T. Hagemeier, A. Buck, and E. Tsotsas, “Experimental measurements of particle collision dynamics in a pseudo-2D gas-solid fluidized bed,” *Chemical Engineering Science*, vol. 167, pp. 297–316, 2017.

[12] OpenCFD, *OpenFOAM: The Open Source CFD Toolbox. User Guide Version 1.4, OpenCFD Limited*. Reading UK, 2007.

[13] I. Demirdzic, Z. Lilek, and M. Peric, “A collocated finite volume method for predicting flows at all speeds,” *International Journal for Numerical Methods in Fluids*, vol. 16, pp. 1029–1050, 1993.

[14] N.-S. Cheng, “Comparison of formulas for drag coefficient and settling velocity of spherical particles,” *Powder Technology*, vol. 189, no. 3, pp. 395–398, 2009.

[15] J. Ding and D. Gidaspow, “A bubbling fluidization model using kinetic theory of granular flow,” *AIChE Journal*, vol. 36, no. 4, pp. 523–538, 1990.